Mechanical performance and fracture behavior of $Fe_{41}Co_7Cr_{15}Mo_{14}Y_2C_{15}B_6$ bulk metallic glass

Q.J. Chen
School of Materials Science and Engineering, Harbin Institute of Technology, Harbin 150001, People's Republic of China; and Department of Materials and Process Engineering, The University of Waikato, Hamilton, New Zealand

J. Shen[a)]
School of Materials Science and Engineering, Harbin Institute of Technology, Harbin 150001, People's Republic of China

D.L. Zhang
Department of Materials and Process Engineering, The University of Waikato, Hamilton, New Zealand

H.B. Fan and J.F. Sun
School of Materials Science and Engineering, Harbin Institute of Technology, Harbin 150001, People's Republic of China

(Received 7 June 2006; accepted 18 September 2006)

The mechanical properties of a new $Fe_{41}Co_7Cr_{15}Mo_{14}Y_2C_{15}B_6$ bulk glassy alloy were studied by impact bending, compression, and hardness tests carried out at room temperature. The compressive fracture strength, elastic strain to fracture, Young's modulus and Vickers hardness were measured to be 3.5 GPa, 1.5%, 265 GPa, and 1253 kg mm^{-2}, respectively. The fracture mode of the glassy alloy under uniaxial compression is different from those of other bulk metallic glasses in that this fracture mode causes the samples to be broken, in an exploding manner, into a large number of micrometer-scale pieces. The fracture mechanisms of this bulk glassy alloy under bending and uniaxial compression are discussed based on the observation of the fracture surfaces. Vickers indentation tests indicate that the structure of the glassy ingot may be inhomogeneous.

I. INTRODUCTION

Recently, the mechanical behavior of Cu-based,[1–3] Zr-based,[4–6] and Pd-based[7,8] bulk metallic glasses (BMGs) has been investigated extensively. However, little research has been reported on the mechanical properties of Fe-based BMGs, mainly because only recently Fe-based BMGs with high glass-forming ability (GFA)[9–13] have been developed. Understanding their mechanical behavior is becoming increasingly important because the high strength and potential low cost of Fe-based BMGs make them attractive for use as advanced engineering materials.

The fracture behavior of BMGs can be classified into two categories based on previous studies: ductile fracture, which has been observed, for example, in ZrCu-based,[14] Pt-based,[15] and Cu-based[16] BMGs; and brittle fracture, which has been observed in Fe-based,[12,13] Mg-based,[17] and Y-based[18] BMGs. In this work, the mechanical behavior of a new Fe-based BMG possessing the highest GFA among Fe-based BMGs discovered so far has been studied to gain insight into the fracture mechanisms of this Fe-based BMG alloy.

II. EXPERIMENTAL PROCEDURE

BMG rods with a composition of $Fe_{41}Co_7Cr_{15}Mo_{14}Y_2C_{15}B_6$were obtained by arc melting a mixture of pure elements Fe, Co, Cr, Mo, Y, C, and FeB pieces in a Ti-gettered argon atmosphere and drop casting the liquid alloy, using its own gravity, into a copper mold 3 mm in diameter. The samples for compression tests had dimensions of 6-mm length and 3-mm diameter and were sliced from the as-cast rods. Both ends of the cylindrical samples were ground and polished to make them flat and parallel. Uniaxial compression tests were performed with a crosshead speed of 0.5 mm/s using an Instron (Norwood, MA) 5500 testing machine. Impact bending tests were carried out by fixing one end of a sample in a vise and impacting the sample along the transverse direction at a point 5 mm above the fixed end. Also, nanoindentation tests were carried out with a maximum load of 2000 kN using a Nano Indenter XP machine (MTS NanoInstruments, Oak Ridge, TN), and

[a)]Address all correspondence to this author.
e-mail: junshen@hit.edu.cn
DOI: 10.1557/JMR.2007.0038

Vickers hardness tests were performed with a load of 5 kg on a model HVS-1000 microhardness instrument (Laizhou Huayin Testing Instrument Co., Ltd., Shandong, P.R. China). The fracture surfaces produced in the compression and bending tests as well as the indents produced in the hardness tests were examined using a Hitachi (Tokyo, Japan) S-4000 scanning electron microscope (SEM) operated at 20 kV and an Olympus BX-51 optical microscope (Center Valley, PA).

III. RESULTS AND DISCUSSION

Figure 1 shows a typical compressive stress–strain curve of the as-cast $Fe_{41}Co_7Cr_{15}Mo_{14}Y_2C_{15}B_6$ BMG sample. This amorphous alloy exhibits an average fracture strength of 3.5 GPa and an average elastic strain to fracture of 1.5%, with no plastic strain prior to failure. This shows that the $Fe_{41}Co_7Cr_{15}Mo_{14}Y_2C_{15}B_6$ BMG is brittle at room temperature. Figure 2(a) shows a typical load–displacement (*P-h*) curve obtained by loading and unloading during nanoindentation test. From Fig. 2(a) it can be seen that the elastic part of the total displacement during loading (h_e) is 390 nm, which is approximately 1/4 of the total displacement. This observation agrees well with values of other Fe-based BMGs.[10] It is worth mentioning that the loading section of the load–displacement curve does not exhibit the pop-in phenomenon, which is often seen in other BMG alloys.[19] This shows that there is no indication of plastic deformation during loading. Figure 2(b) shows the hardness as a function of depth measured by the nanoindentation tests. It can be seen that the measured hardness decreases with increasing indentation depth up to 500 nm and then remains constant. The initial variation of the measured hardness with indentation depth might result from work hardening caused by polishing of the sample surface. The hardness measured from Vickers hardness test is 1253 Kg mm^{-2}. As shown in Table I, the elastic strain to fracture, Vickers hardness, compression fracture strength, and nanoindentation hardness of the $Fe_{41}Co_7Cr_{15}Mo_{14}Y_2C_{15}B_6$ BMG are similar to those of other Fe-based BMGs with high GFA.

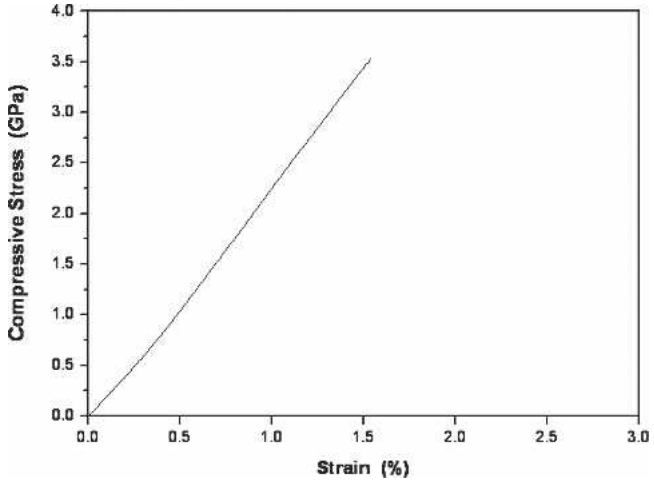

FIG. 1. Compression stress–strain curve of $Fe_{41}Co_7Cr_{15}Mo_{14}C_{15}B_6Y_2$ bulk amorphous alloy.

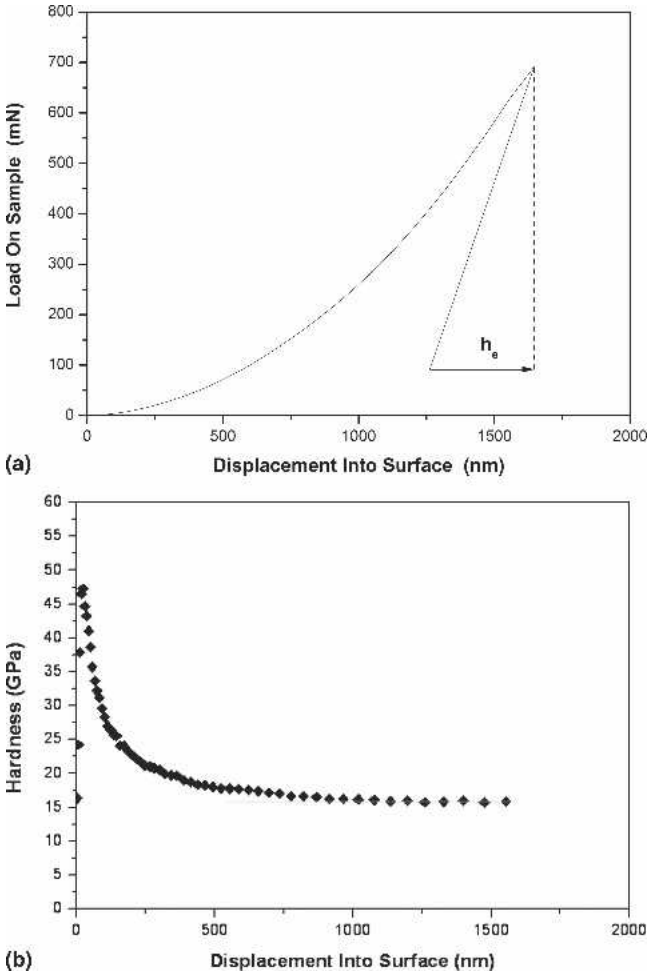

FIG. 2. Nanoindentation of $Fe_{41}Co_7Cr_{15}Mo_{14}C_{15}B_6Y_2$ bulk amorphous alloy: (a) curve of load versus displacement and (b) curve of hardness versus displacement.

During bending impact tests, the samples broke along an angle of approximately 57° with respect to the axis of sample, as shown in Fig. 3(a). The fracture surface consists of a mixture of smooth and coarse regions, which result from shear and tear stresses, respectively, as shown in Fig. 3(b). It is well known that the fracture surface of glassy ceramic contains four regions: source of failure, smooth mirror region, mist region, and hackle region.[21] The smooth mirror region is highly reflective to light and the mist and hackle regions contain microcracks and large secondary cracks, respectively. The fracture surface produced by impact bending the $Fe_{41}Co_7Cr_{15}Mo_{14}Y_2C_{15}B_6$ BMG is similar to that of a glassy ceramic but contains no mist and hackle regions. It appears that the relative magnitude of the shear stress and tear stress along the

TABLE I. Mechanical properties of several Fe-based bulk amorphous alloys.

Alloys	Plastic strain (%)	Elastic strain (%)	Vickers hardness (Kg mm^{-2})	Compression strength (GPa)	Young's modulus (GPa)	Nanoindentation hardness (GPa)
$(Fe_{44.3}Cr_5Co_5Mo_{12.8}Mn_{11.2}C_{15.8}B_{5.9})Y_{1.5}$ [10][a]	0	···	1224	3.0	257.1	14.8
$Fe_{65.5}Cr_4Mo_4Ga_4P_{12}C_5B_{5.5}$ [20][a]	0.3	1.6	885	2.8	161.0	···
$Fe_{41}Co_7Cr_{15}Mo_{14}Y_2C_{15}B_6$	0	1.5	1253	3.5	265.1	15.9

[a]The numbers in brackets are references.

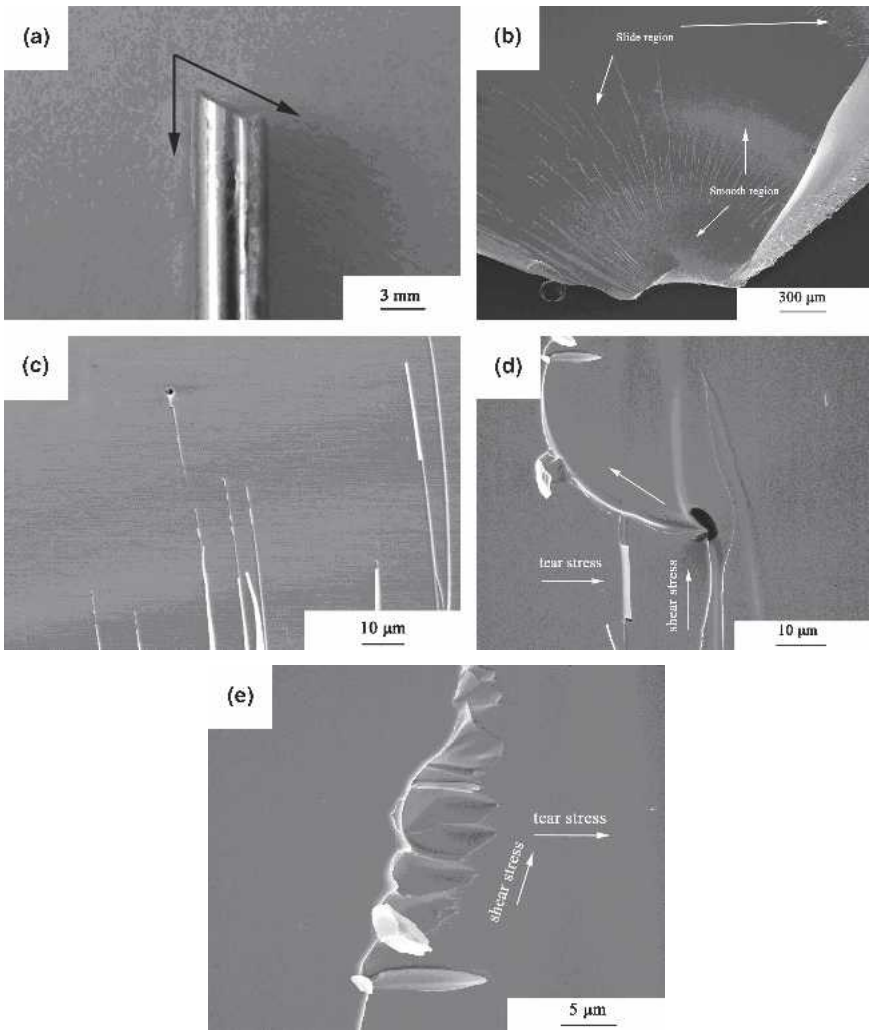

FIG. 3. Bend fracture morphology of $Fe_{41}Co_7Cr_{15}Mo_{14}C_{15}B_6Y_2$ bulk amorphous alloy 3 mm in diameter showing (a) bending fracture surface, (b) general fracture morphology, (c) block of shear band, (d) deflection of shear band, and (e) ductile pit.

fracture surface varies as the crack propagates during fracture. In the initial stage of fracture, the shear stress is dominant, and this results in a smooth fracture surface. With the further propagation of the crack, the tearing stress becomes dominant, and this causes an increase in the number of shear bands and results in a fracture surface with slip lines. With the increase of stress, many new surfaces were produced to accommodate more stress. Nucleation of cracks occurs when the density of the shear bands is high enough and the propagation of shear bands is blocked by their intersection with each other; then crack growth proceeds until the final fracture.

It was also observed that some shear bands were blocked by the pores existing in the specimen [Fig. 3(c)], and some were deflected by the pores [Fig. 3(d)]. This demonstrates that the presence of defects such as pores in the as-cast BMG bar increases the complexity of the development of shear bands. Further examination of the fracture surfaces also revealed some dimples aligned in the direction of shear stress [Fig. 3(e)]. These dimples are

similar to the dimples formed in the hackle bands on the fracture surface of polymer materials.[21] It is likely that these dimples result from the combined effects of the shear stress and the tear stress. Overall, it can be concluded that the fracture surfaces produced by impact bending of the $Fe_{41}Co_7Cr_{15}Mo_{14}Y_2C_{15}B_6$ BMG bars have features that can be found on the fracture surfaces of glassy ceramic and polymer materials, and the shear bands are characteristic of bulk metallic glasses.

It was discovered that the fracture mode of the $Fe_{41}Co_7Cr_{15}Mo_{14}Y_2C_{15}B_6$ BMG during compression tests was dramatically different from that of other BMGs reported so far. It has been reported in literature that during uniaxial compression tests, the fracture of bulk metallic glassy alloys such as Zr-based,[14] Pd-based,[15] and Cu-based[16] alloys occurs along a single plane with an angle less than 45° with respect to the loading axis. The fracture of brittle Fe-based[13] and Mg-based[17] BMGs does not occur along a single flat plane, but the number of fracture planes is still very limited. However, in this study it was found that the samples of $Fe_{41}Co_7Cr_{15}Mo_{14}Y_2C_{15}B_6$ BMG were broken into a large number of small and sharp pieces with sizes in the range of 30–200 μm during compression tests, as shown in Fig. 4(a). This observation shows that under sufficiently high stress, a large number of cracks nucleate and propagate simultaneously along various separate planes. SEM examination of the pieces shows that there are a number of shear bands on the fracture surfaces [Fig. 4(b)], which indicates that the localized plastic deformation by shear banding occurs on a microscopic scale in the specimen before final fracture. Occasionally, the cracks [as indicated by arrows in Fig. 4(c)] can be seen on the fracture surfaces. Figure 4(d) shows that the shear bands on one plane are intercepted by shear bands on a neighboring plane, which blocked the propagation of shear bands and led to the increase of local density of shear bands. It is expected that shear band interception would result in stress concentration, which promotes the nucleation and growth of cracks at the intersection sites [Fig. 4(e)].

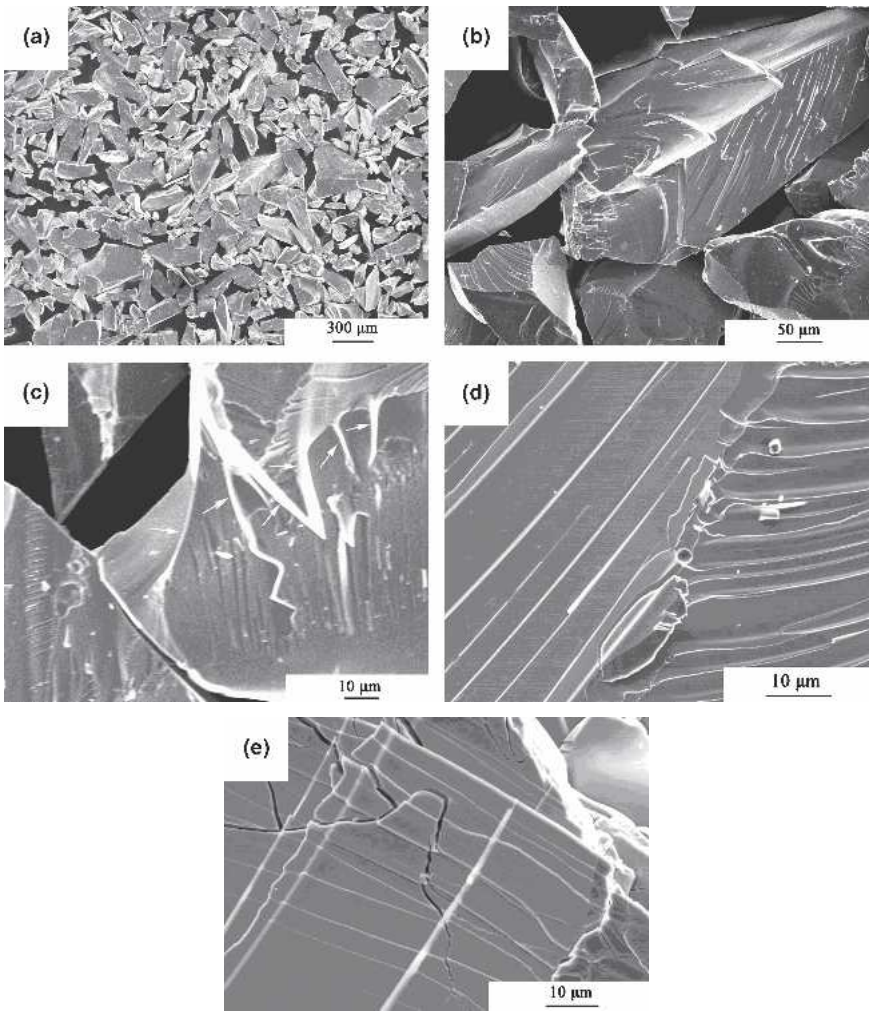

FIG. 4. SEM images of compression fracture morphologies of $Fe_{41}Co_7Cr_{15}Mo_{14}C_{15}B_6Y_2$ bulk amorphous alloy showing (a) outer morphologies of compression fractured pieces, (b) shear bands on fracture surfaces, (c) cracks, (d) intersection of shear bands, and (e) extension of cracks.

The fracture mode of the $Fe_{41}Co_7Cr_{15}Mo_{14}Y_2C_{15}B_6$ BMG under compression and the features of the fracture surfaces provide some insight into the fracture mechanisms of brittle BMGs under uniaxial compression. In the fully amorphous specimens, some pores and free volumes are formed during solidification of the viscous supercooled liquids, as shown schematically in Fig. 5(a). Under compression, stress concentration is likely to arise at these pores and free volumes, and thus they can become the origins for formation of microcracks. At the same time, free volumes may coalescence to form cavities under compression. With increasing compressive loading, the local shear stress around the defects will increase to be greater than the yield strength of the BMG and thus induce shear bands, as shown schematically in Fig. 5(b). When the stress is further increased, the density of shear bands rapidly increases, and the shear bands from neighboring planes start to intercept each other, resulting in an increase of stress concentration and promotion of nucleation and growth of numerous cracks [Fig. 5(c)]. Finally, the specimen breaks into a large number of small pieces [Fig. 5(d)].

To further investigate the mechanical behavior of this new bulk amorphous alloy, Vickers indentation tests were conducted at different locations on the transverse section of the as-cast rod using a load of 500 g. The morphology of the indents was examined using an optical microscope (Fig. 6). It was observed that there were some shear bands around the indents produced at locations close to the outskirts of the specimen [Fig. 6(a)], but there were no shear bands around the indents produced in the areas between the outskirts and center of the transverse section of the specimen [Fig. 6(b)]. Interestingly, cracks appeared around each of the indents produced near the center of the transverse section [Fig. 6(c)]. This observation indicates that the as-cast rod of the new Fe-based bulk metallic glass may have an inhomogeneous structure due to the variation of cooling rates in different sections of the specimen along the radial direction.

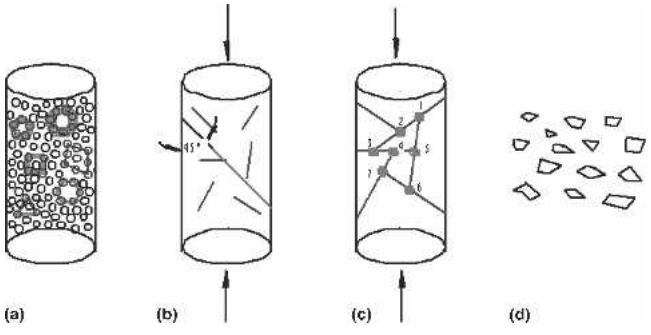

FIG. 5. Sketch of compression fracture process of $Fe_{41}Co_7Cr_{15}Mo_{14}C_{15}B_6Y_2$ bulk amorphous alloy: (a) origin of cracks, (b) propagation of cracks, (c) intersection of cracks, and (d) compressive fractured pieces.

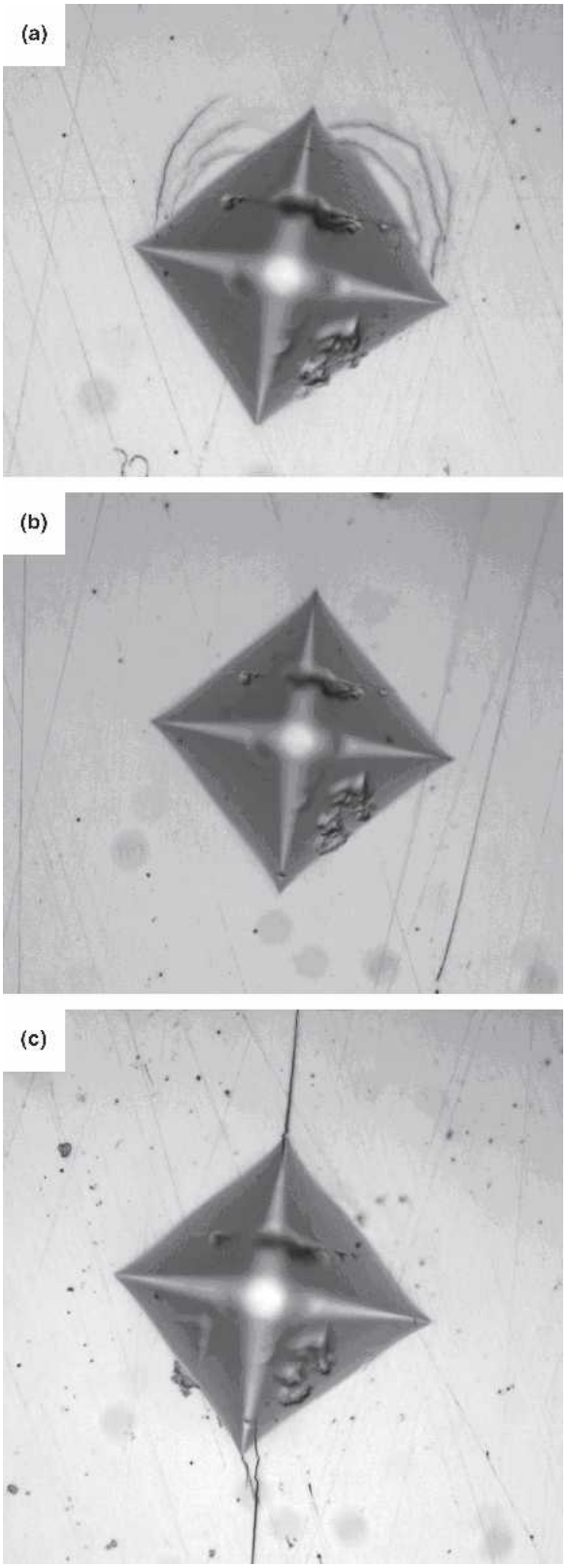

FIG. 6. Indentation morphology for different positions of $Fe_{41}Co_7Cr_{15}Mo_{14}C_{15}B_6Y_2$ bulk amorphous alloy showing: (a) shear band (outer), (b) no shear band (between the outskirts and the center of the specimen), and (c) crack (center).

IV. CONCLUSION

The $Fe_{41}Co_7Cr_{15}Mo_{14}Y_2C_{15}B_6$ bulk metallic glass has a high compressive fracture strength of 3500 MPa, a high Vickers hardness of 1253 Kg mm^{-2}, and a high elastic modulus of 265 GPa. The fracture mode of this Fe-based BMG under uniaxial compression is such that the samples are broken into a large number of small micrometer-scale pieces in an exploding fashion. There is no evidence of macroscopic plastic deformation, but formation and intersection of shear bands are evident on the fractured surfaces of the broken pieces and around the indents produced near the surface of the sample, suggesting that localized plastic deformation occurs at the microscopic scale. It appears that the structure of the glassy alloy is inhomogeneous resulting from variation of cooling rates in solidification of the material.

ACKNOWLEDGMENTS

This work was supported by the Program for New Century Excellent Talents in University (China). The authors would also thank the Asia 2000 Foundation in New Zealand for partially funding this collaborative work.

REFERENCES

1. W. Zhang and A. Inoue: Cu-based bulk glass formation in the Cu–Zr–Ga alloy system and their mechanical properties. *Mater. Trans.* **45,** 532 (2004).
2. P. Wesseling, T.G. Nieh, W.H. Wang, and J.J. Lewandowski: Preliminary assessment of flow, notch toughness, and high temperature behavior of $Cu_{60}Zr_{20}Hf_{10}Ti_{10}$ bulk metallic glass. *Scripta Mater.* **51,** 151 (2004).
3. M. Calin, J. Echert, and L. Schultz: Improved mechanical behavior of Cu–Ti-based bulk metallic glass by in situ formation of nanoscale precipitates. *Scripta Mater.* **63,** 653 (2003).
4. Z.F. Zhang, J. Echert, and L. Schultz: Difference in compressive and tensile fracture mechanisms of $Zr_{59}Cu_{20}Al_{10}Ni_8Ti_3$ bulk metallic glass. *Acta Mater.* **51,** 1167 (2003).
5. C.J. Gilbert, R.O. Ritchie, and W.L. Johnson: Fracture toughness and fatigue-crack propagation in a Zr–Ti–Ni–Cu–Be bulk metallic glass. *Appl. Phys. Lett.* **71,** 476 (1997).
6. Z.F. Zhang, J. Echert, and L. Schultz: Tensile and fatigue fracture mechanisms of a Zr-based bulk metallic glass. *J. Mater. Res.* **18,** 456 (2003).
7. C.L. Ma and A. Inoue: Deformation and fracture behaviors of Pd–Cu–Ni–P glassy alloys. *Mater. Trans.* **43,** 3266 (2002).
8. T. Mukai, T.G. Nieh, Y. Kawamura, A. Inoue, and K. Higashi: Effect of strain rate on compressive behavior of a $Pd_{40}Ni_{40}P_{20}$ bulk metallic glass. *Intermetallics* **10,** 1071 (2002).
9. V. Ponnambalam, S.J. Poon, and G.J. Shiflet: Fe-based bulk metallic glasses with diameter thickness larger than one centimeter. *J. Mater. Res.* **19,** 1320 (2004).
10. Z.P. Lu, C.T. Liu, J.R. Thompson, and W.D. Porter: Structure amorphous steels. *Phys. Rev. Lett.* **92,** 245503-1 (2004).
11. J. Shen, Q.J. Chen, J.F. Sun, H.B. Fan, and G. Wang: Exceptionally high glass-forming ability of FeCoCrMoCBY alloys. *Appl. Phys. Lett.* **86,** 151907-1 (2005).
12. Q.J. Chen, H.B. Fan, L. Ye, S. Ringer, J.F. Sun, J. Shen, and D.G. McCartney: Enhanced glass forming ability of Fe–Co–Zr–Mo–W–B alloys with Ni addition. *Mater. Sci. Eng., A* **402,** 188 (2005).
13. A. Inoue, B.L. Shen, A.R. Yavari, and A.L. Greer: Mechanical properties of Fe-based bulk glassy alloys in Fe–B–Si–Nb and Fe–Ga–P–C–B–Si systems. *J. Mater. Res.* **18,** 1487 (2003).
14. J. Das, M.B. Tang, K.B. Kim, R. Theissmann, F. Baier, W.H. Wang, and J. Eckert: "Work-hardenable" ductile bulk metallic glass. *Phys. Rev. Lett.* **94,** 205501-1 (2005).
15. J. Schroers and W.L. Johnson: Ductile bulk metallic glasses. *Phys. Rev. Lett.* **93,** 255506-1 (2004).
16. A. Inoue, W. Zhang, T. Zhang, and K. Kurosaka: High-strength Cu-based bulk glassy alloys in CuZrTi and CuHfTi ternary systems. *Acta Mater.* **49,** 2645 (2001).
17. X.K. Xi, D.Q. Zhao, M.X. Pan, W.H. Wang, Y. Wu, and J.J. Lewandowski: Fracture of brittle metallic glasses: Brittleness or plasticity. *Phys. Rev. Lett.* **94,** 125510 (2005).
18. F.Q. Guo, P.J. Poon, and G.J. Shiflet: Metallic glass ingots based on yttrium. *Appl. Phys. Lett.* **83,** 2575 (2003).
19. C.A. Schuh and T.G. Nieh: A nanoindentation study of serrated flow in bulk metallic glasses. *Acta Mater.* **51,** 87 (2003).
20. M. Stoica, J. Echert, S. Roth, Z.F. Zhang, L. Schultz, and W.H. Wang: Mechanical behavior of $Fe_{65.5}Cr_4Mo_4Ga_4P_{12}C_5B_{5.5}$ bulk metallic glass. *Intermetallics* **13,** 764 (2005).
21. S. Wole: *Mechanical Properties of Engineered Material* (Marcel Dekker New York, 2002), pp. 389, 391.